ingegneria sismica
International Journal of Earthquake Engineering
Anno XLIII - Num. 3 - 2026

Research on Distributed Photovoltaic Site Selection and Capacity Determination Based on Maximizing Distribution Network Benefits

Hongyu Su[1] *and Zhisheng Zhang*[1,*]

[1] College of Electrical Engineering of Qingdao University, Qingdao 266071, Shandong, China

Abstract: The large-scale integration of distributed photovoltaic (DPV) into distribution networks brings significant low-carbon benefits, but also poses new challenges to the safe and economic operation of distribution networks. As the direct carrier of DPV grid connection, distribution networks need to balance system security, operational economy and low-carbon emission reduction in the planning process, and the access location and capacity of DPV directly affect the realization of these goals. Therefore, how to scientifically plan the access scheme of DPV from the perspective of distribution networks to maximize its comprehensive benefits has become a key issue that needs to be urgently addressed. To this end, this paper proposes a DPV siting and sizing planning model aimed at maximizing the comprehensive benefits of distribution networks. Firstly, Latin hypercube sampling (LHS) and fast forward elimination techniques are used to handle the randomness of DPV output and generate typical output scenarios. Secondly, the investment return of DPV independent power producers (DPV-IPP) is taken as the economic evaluation index, and a comprehensive benefit model of distribution networks including annual grid loss profit and loss, annual voltage quality profit and loss and annual carbon emission reduction benefits is established. The genetic algorithm is used to solve the above model and jointly optimize the location and capacity of DPV. Finally, a case study is conducted on the IEEE-33 node distribution system to verify that the model can provide a scientific decision-making basis for distribution network operators in DPV planning.

Key words: Distributed Photovoltaic; Distribution Network; Carbon Emission Reduction; Independent Power Producer; Site Selection and Capacity Determination

1 Introduction

Population growth and economic development have driven up the demand for electricity and global energy consumption. At the same time, the depletion of traditional fossil fuels and the increasing need for carbon emission reduction have made the development of renewable energy generation technologies an urgent priority. Distributed photovoltaic (DPV) has attracted much attention due to its environmental friendliness, reliability and flexibility [1]. The integration of DPV into distribution networks will affect node voltages, line power flows, etc., and the extent of such impacts is closely related to the access location and capacity [2]. To fully leverage the benefits of DPV and minimize its negative effects, it is necessary to rationally plan the layout of DPV in the planning stage.

With the in-depth advancement of the "dual carbon" goals, the objective of DPV siting and sizing planning research is no longer confined to the economy and reliability of the distribution network, but has expanded to simultaneously consider economy, reliability, and

*slnzzs@126.com
https://doi.org/10.65102/is20261042 Published: 10 June , 2026

environmental protection. Abdulmula et al. [3] proposed a DPV siting and sizing model aimed at minimizing the annual operating cost of the distribution network, with the operating cost including low-carbon environmental protection expenses; George & Venayagamoorthy [4] proposed a two-layer optimization model for DPV siting and sizing considering regional carbon emissions, where the outer layer optimization model's objective takes into account the low-carbon environmental protection rewards and penalties of the distribution network. Compared with traditional DPV siting and sizing planning schemes, the above planning schemes that consider low-carbon environmental protection expenses in the objective function can effectively reduce the system's CO2 emissions. However, current research mostly focuses on low-carbon costs, while considering low-carbon benefits is relatively rare.

With the in-depth advancement of power marketization reform, the traditional planning model of distribution networks is gradually shifting from single-subject decision-making to multi-subject participation [5], and the number of new investment entities such as DPV-IPP is increasing day by day. As the direct carrier for DPV grid connection, the safe and stable operation of distribution networks has always been the basic premise of planning decisions. Especially in regions where natural disasters such as earthquakes occur frequently, as a key infrastructure, the power supply reliability of distribution networks directly affects the regional earthquake resilience and emergency response efficiency. Therefore, most existing studies start from the perspective of distribution networks. However, these studies rarely consider the impact of planning schemes on the economic benefits of DPV-IPP.

In summary, in the current research on DPV site selection and capacity planning, there is a general lack of consideration for the economic viability of DPV-IPP and the inclusion of low-carbon benefits in the planning objectives. Therefore, this paper first addresses the randomness of DPV output [6] by using Latin hypercube sampling (LHS) technology and a fast forward elimination technique based on probability distance to process the DPV output model and generate typical output scenarios. Secondly, an optimization model is established with the goal of maximizing the comprehensive benefits of the distribution network, and the investment returns of DPV-IPP are used as economic evaluation indicators. Thirdly, the genetic algorithm (GA) is adopted to solve the model. Finally, a case study is conducted using the IEEE-33 node distribution system to verify the effectiveness of the proposed model.

2 Scene generation and scene reduction

2.1 DPV Uncertainty Modeling

The output power of DPV is closely related to environmental factors, mainly affected by the local light intensity [7]. In this paper, the variation of solar light intensity within a certain period of time is represented by the Beta distribution, whose probability density function is expressed as [8]:

$$f(r)=\frac{\Gamma(\alpha+\beta)}{r_{\max}\Gamma(\alpha)\Gamma(\beta)}\left(\frac{r}{r_{\max}}\right)^{\alpha-1}\left(1-\frac{r}{r_{\max}}\right)^{\beta-1} \tag{1}$$

where, r represents the intensity of sunlight within a certain period of time; $r_{\max}$ represents the maximum value of the light intensity within a certain period of time; α and β are shape parameters of the Beta distribution.

According to relevant research, the magnitude of the DPV output power is determined by the intensity of sunlight and shows a linear relationship. Therefore, the per-unit value of the

DPV output power can be approximately expressed as [9]:

$$P_S = r / r_{max} \tag{2}$$

where, $P_S (0 \le P_S \le 1)$ is the per-unit value of the output power of the DPV.

From Equations (1) and (2), the probability density function of the DPV output power can be obtained as [10]:

$$f(P_S) = \frac{\Gamma(\alpha+\beta)}{\Gamma(\alpha)\Gamma(\beta)} P_S^{\alpha-1}(1-P_S)^{\beta-1} \tag{3}$$

2.2 Latin hypercube sampling

LHS is a stratified sampling method that provides more uniform coverage of the input space, higher statistical accuracy, and ensures the comprehensiveness of the sample results. The schematic diagram of LHS is shown in Figure 1. Suppose a random variable is sampled N times. LHS divides the vertical axis of its cumulative distribution function into N equal intervals, randomly selects a random number y_i in each interval as the sampling value, and maps y_i to the sampling value x_{mn} through the inverse function F_m^{-1} of the cumulative probability density function. The value of x_{mn} can be expressed as [11]:

$$x_{mn} = F_m^{-1}(y_i) \tag{4}$$

After sampling all the random variables, the sampling matrix $\boldsymbol{A}$ of order $M \times N$ can be obtained.

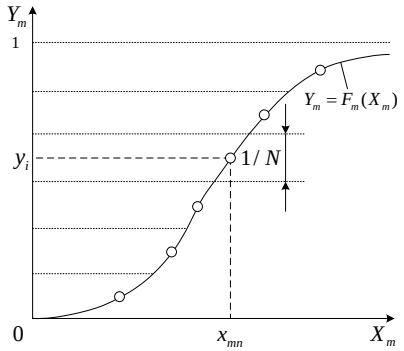

Figure 1: Schematic diagram of LHS

2.3 Fast forward elimination technique based on probability distance

Theoretically, the larger the scale of the scenario and the higher the simulation accuracy, the lower the computational efficiency will be, and the complexity of solving the optimization model will be significantly increased. To balance the accuracy and computational load, this paper adopts a fast forward elimination technique based on probability distance [12] to reduce the similar scenarios in the scenario set S generated by LHS. Only a few most typical scenarios are selected to participate in the later calculation. The basic steps are as follows:

Step 1: Calculate the Euclidean norm $s(c_i, c_j)$ between every two scenes (c_i, c_j) in the set S, as shown in Equation (5):

$$s(c_i, c_j) = \| c_i - c_j \| = \sqrt{\sum_{l=1}^{24\times500} (c_i^l - c_j^l)^2} \tag{5}$$

where, c_i^l and c_j^l are respectively the l-th values in the i-th and j-th scenarios.

Step 2: Assume that the probability p of each scenario occurring is the same;

Step 3: Identify the set of all the minimum values of the product of the Euclidean norm of each pair of scenes (c_n, c_m) and the occurrence probability $p^{(n)}$ of scene c_n in all scenarios, and denote it as set D, as shown in Equation (6) [13]:

$$D = \left\{ \min_{n\in\{1,2,\ldots,S\}, n\neq m} p^{(n)} s(c_n, c_m) \right\} \tag{6}$$

Step 4: Based on Step 3, reduce a certain number of scenarios c_{s^*} that satisfy Equation (7):

$$p^{(s^*)} p^{(s)} \min_{s\neq s^*} s(c_s, c_{s^*}) = \min_{m\in\{1,2,\ldots,S\}} p^{(m)} D \tag{7}$$

where, $p^{(s^*)}$ is the probability of the reduced scenario c_{s^*}; $p^{(m)}$ is the probability of scenario c_m.

Step 5: Find the scenario with the smallest probability distance to the reduced scenario, and update its probability to be equal to the sum of its original probability and the probability of the reduced scenario. Finally, update the elements in the scenario set D;

Step 6: Repeat steps 2 to 5. If the remaining number of scenarios is met, stop the operation; otherwise, continue to reduce.

3 DPV Optimization Configuration Model

The in-depth advancement of the "dual carbon" goals has put forward higher requirements for the low-carbon operation of distribution networks. Meanwhile, the connection of DPV will have a significant impact on the network loss, node voltage, and carbon emissions of distribution networks. As the direct carrier for the grid connection of DPV, distribution networks must ensure the safe operation of the system, make scientific decisions on the connection location and capacity of DPV, and strive to maximize their own comprehensive benefits. At the same time, as an important investment entity, the investment returns of DPV-IPP are also an important dimension for evaluating the economic rationality of planning schemes [14]. Therefore, this paper starts from the perspective of distribution networks and establishes an optimization model with the maximization of the comprehensive benefits of distribution networks as the objective, and takes the investment returns of DPV-IPP as the economic evaluation index. Figure 2 sorts out the decision and evaluation relationship between distribution networks and DPV-IPP.

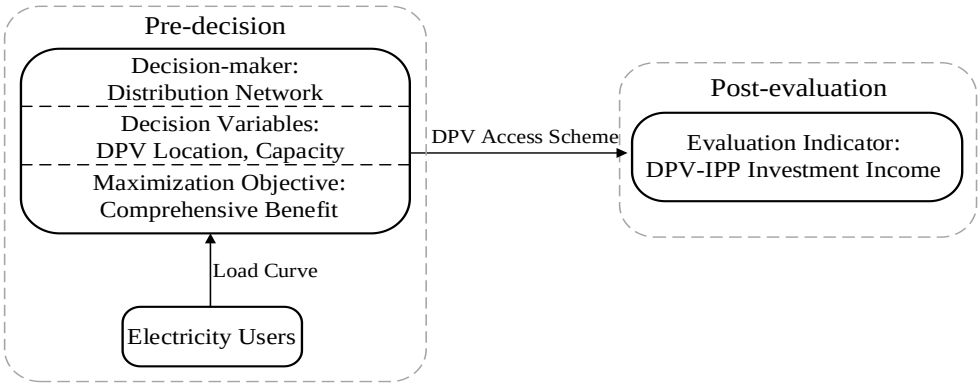

Figure 2: Schematic Diagram of the Decision-Evaluation Relationship

3.1 Objective function

Existing studies on the emission reduction capacity of distribution networks mostly incorporate carbon emission costs into the total cost without considering it as an independent revenue item. Therefore, this paper includes carbon emission reduction revenues in the revenue of distribution networks and constructs a comprehensive revenue model from three aspects: system line loss, voltage quality, and carbon emissions [15]. The comprehensive revenue of the distribution network is represented by the sum of the annual grid loss profit and loss (C_{Ploss}), the annual voltage quality profit and loss (C_{voltage}), and the annual carbon emission reduction revenue (C_{carbon}):

$$\max C_{DN} = C_{\text{Ploss}} + C_{\text{voltage}} + C_{\text{carbon}} \tag{8}$$

(1) The annual grid loss profit and loss

C_{Ploss} refers to the difference in system network loss costs before and after the installation of DPV, that is, $C_{\text{Ploss}} = C_{\text{s}}^{\text{before}} - C_{\text{s}}^{\text{after}}$. Among them, the calculation formula for system network loss cost C_{s} is [16]:

$$C_{\text{s}} = p\sum_{m=1}^{M} D_m \left(\sum_{t=1}^{T}\left(\sum_{i,j\in N} I_{ij}^2(t)R_{ij}\right)\right) \tag{9}$$

where, p represents the electricity selling price; M is the number of typical day types within the planning year; D_m is the number of typical days of the m-th type within the planning year; T is the number of time periods within a typical day; N represents the number of nodes in the distribution network; $I_{ij}(t)$ is the current of line ij at time t; R_{ij} is the impedance of line ij.

(2) The annual voltage quality profit and loss

The connection of DPV has a significant impact on the system voltage. This paper quantifies this effect through the annual voltage quality profit and loss (C_{voltage}). When DPV is connected and the voltage quality is improved, avoiding power quality fines, equipment losses, and user complaint losses, $C_{\text{voltage}} > 0$, indirect benefits are generated; conversely, $C_{\text{voltage}} < 0$. The calculation formula is [17]:

$$\Delta C_{\mathrm{U}} = (\frac{\lambda_{\mathrm{before}}}{\lambda_{\mathrm{after}}} - 1) C_{\mathrm{imu}} \tag{10}$$

$$\lambda = \sum_{m=1}^{M} D_m (\sum_{i=1}^{N} U_{m,i} P_{\mathrm{L},m,i} k_i) \tag{11}$$

where, λ is the system voltage index; $\lambda_{\mathrm{before}}$ and λ_{after} represent the system voltage indicators before and after the installation of DPV; C_{imu} is the annual benefit that the power grid gains for each one-percentage-point improvement in system voltage quality; $U_{m,i}$ is the voltage magnitude of node i in the m-th type of typical day; $P_{\mathrm{L},m,i}$ is the load of node i in the m-th type of typical day; k_i is the weight of each node.

(3) The annual carbon emission reduction revenue

Assuming all non-DPV electricity in the distribution network is supplied by coal-fired units from the main grid, C_{carbon} equals the carbon reduction revenue from fossil fuel savings due to DPV integration during the planning period. The formula is as follows [18]:

$$C_{\mathrm{H}} = \sum_{m=1}^{M} D_m (\sum_{t=1}^{T} (\sum_{i=1}^{N} c_1 \varepsilon P_{\mathrm{pv},m,t,i})) \tag{12}$$

where, c_1 represents the real-time price of the carbon trading market; ε represents the coefficient of carbon dioxide emissions per unit of electricity generated by coal-fired power units; $P_{\mathrm{pv},m,t,i}$ is the power generation of the DPV at node i at time t on the m_th type typical day.

3.2 Economic evaluation index

To comprehensively evaluate the impact of different planning schemes on DPV-IPP, this paper introduces the investment return of DPV-IPP (C_{IPP}) as an economic evaluation index. This indicator reflects the annual income level of DPV-IPP per unit investment, and its calculation formula is shown in Equations (13) to (17) [19]:

$$C_{\mathrm{IPP}} = \frac{C_{\mathrm{TPF}}}{C_{\mathrm{INV}}} \tag{13}$$

where, C_{TPF} and C_{INV} represent the annualized investment income and investment cost of DPV.

C_{TPF} includes the revenue from DPV power sales and policy subsidies obtained due to the use of renewable energy or environmental improvement, etc. Among them, the DPV power generation adopts the "surplus power to grid" model [20]. For the self-consumption of DPV, there is a subsidy on the basis of the electricity price; for the reverse feed-in to the grid of DPV, it is purchased at the local desulfurization electricity price plus subsidy. Its mathematical model is:

When the power generation of DPV is less than the load demand, the investment return of DPV-IPP is:

$$C_{\mathrm{TPF}}=\sum_{m=1}^{M}D_m(\sum_{t=1}^{T}(\sum_{i=1}^{N_{\mathrm{pv}}}(p+p_{\mathrm{en}})P_{\mathrm{pv},m,t,i})) \tag{14}$$

where, p_{en} represents the government's photovoltaic subsidy electricity price; M is the number of typical day types within the planning year; D_m is the number of typical days of the m-th type within the planning year; T is the number of time periods within a typical day; N_{pv} is the number of DPV installation nodes.

When the power generation of DPV is more than the load demand, the investment return of DPV-IPP is [21]:

$$C_{\mathrm{TPF}}=\sum_{m=1}^{M}D_m(\sum_{t=1}^{T}(\sum_{i=1}^{N_{\mathrm{pv}}}c_{\mathrm{TPF}})) \tag{15}$$

$$c_{\mathrm{TPF}}=(p+p_{\mathrm{en}})P_{\mathrm{L},m,t,i}+(p+p_{\mathrm{sell}})(P_{\mathrm{pv},m,t,i}-P_{\mathrm{L},m,t,i}) \tag{16}$$

where, p_{sell} represents the desulfurization electricity price of the power grid; $P_{\mathrm{L},m,t,i}$ represents the load at node i at time t in the m_th type of typical day.

C_{INV} refers to the construction and installation costs as well as the operation and maintenance costs of investing in DPV. Its mathematical model is:

$$C_{\mathrm{INV}}=c_2\sum_{i=1}^{N}(\frac{r(r+1)^y}{(1+r)^y-1}S_{\mathrm{pv},i})+c_3\sum_{m=1}^{M}D_m(\sum_{t=1}^{T}(\sum_{i=1}^{N}P_{\mathrm{pv},m,t,i})) \tag{17}$$

where, c_2 and c_3 represent the unit investment cost and the unit operation and maintenance cost per unit capacity of DPV; $S_{\mathrm{pv},i}$ is the rated installed capacity of DPV at node i; r is the discount rate; y is the planning period of DPV.

3.3 Constraints

The constraints include:

(1) Power balance constraint

$$\begin{cases} P_{\mathrm{S},i}+P_{\mathrm{pv},i}-P_{\mathrm{L},i}-U_i\sum_{j=1}^{N}U_j(G_{ij}\cos\delta_{ij}+B_{ij}\sin\delta_{ij})=0 \\ Q_{\mathrm{S},i}+Q_{\mathrm{pv},i}-Q_{\mathrm{L},i}-U_i\sum_{j=1}^{N}U_j(G_{ij}\cos\delta_{ij}-B_{ij}\sin\delta_{ij})=0 \end{cases} \tag{18}$$

where, $P_{\mathrm{S},i}$ and $Q_{\mathrm{S},i}$ represent the active and reactive power injected by the upper-level power grid at node i; $P_{\mathrm{pv},i}$ and $Q_{\mathrm{pv},i}$ represent the active and reactive power injected by the DPV at node i; $P_{\mathrm{L},i}$ and $Q_{\mathrm{L},i}$ represent the conventional active and reactive loads at node i; U_i represents the magnitude of the node voltage; G_{ij} and B_{ij} represent the system admittance; δ_{ij} represents the phase angle difference of the node voltage.

(2) Node voltage operational constraints

$$U_{\min} \le U_i \le U_{\max} \tag{19}$$

where, $U_{\min}$ and $U_{\max}$ are respectively the lower and upper limits of the node voltage, with their values being $0.95U_N$ and $1.05U_N$, and U_N represents the rated voltage of the system.

(3) Capacity constraints for DPV access

$$0 \le S_{\mathrm{pv},i} \le S_{\mathrm{pv},i}^{\max} \tag{20}$$

where, $S_{\mathrm{pv},i}$ represents the capacity of the DPV connected to node i; $S_{\mathrm{pv},i}^{\max}$ also represents the maximum allowable connection capacity at node i.

4 Model Construction for DPV Site Selection and Capacity Determination

4.1 Genetic Algorithm

GA is a heuristic algorithm based on the principles of natural selection and genetics, simulating the process of biological evolution.

4.1.1 Initialize the population

This paper adopts LHS to initialize the population capacity, ensuring the uniform distribution of solutions in the search space, which is conducive to the algorithm's better exploration of the global solution space.

Heuristic rules [22] generate the initial population by using the prior knowledge of the problem, which can enhance the overall quality of the population and make the initial solution closer to the global optimal solution. Relevant literature indicates that installing photovoltaic systems in areas with high loads can better achieve local consumption, improve the stability and economy of the system [23]. Therefore, in this paper, the population positions are initialized through heuristic rules. Firstly, the weights of each candidate node are calculated based on the load size, taking all candidate nodes as samples, and then a certain number of samples are drawn without replacement according to the weights as the initial position variables.

4.1.2 Crossover operation and mutation operation

In this paper, the Simulated Binary Crossover (SBX) is adopted for generating offspring, and the Polynomial Mutation (PM) is used to mutate the generated offspring individuals [24].

To increase population diversity, a larger distribution index for crossover and mutation is set in the early stage of the algorithm. As the number of iterations increases, the distribution index is gradually reduced to enhance convergence, thereby more accurately finding the optimal solution. Its update formula is [25]:

$$\eta = \frac{\eta_{\mathrm{origin}} GEN}{GEN_{\max}} \tag{21}$$

$$\sigma = \frac{\sigma_{\text{origin}} GEN}{GEN_{\max}} \tag{22}$$

where, η is the cross-distribution index; σ is the mutation-distribution index; η_{origin} and σ_{origin} are the initial values of η and σ; GEN represents the current iteration count; $GEN_{\max}$ is the maximum number of iterations.

4.2 Model solving process

Based on the grid structure of the distribution network, input typical scenarios of photovoltaic and basic load, set constraints such as the access capacity of DPV, and use GA to optimize and solve the model [26]. Finally, output the optimal planning scheme of DPV, and the optimal scheme obtained includes the access nodes of each DPV and the corresponding installation capacity. The specific solution process is shown in Figure 3:

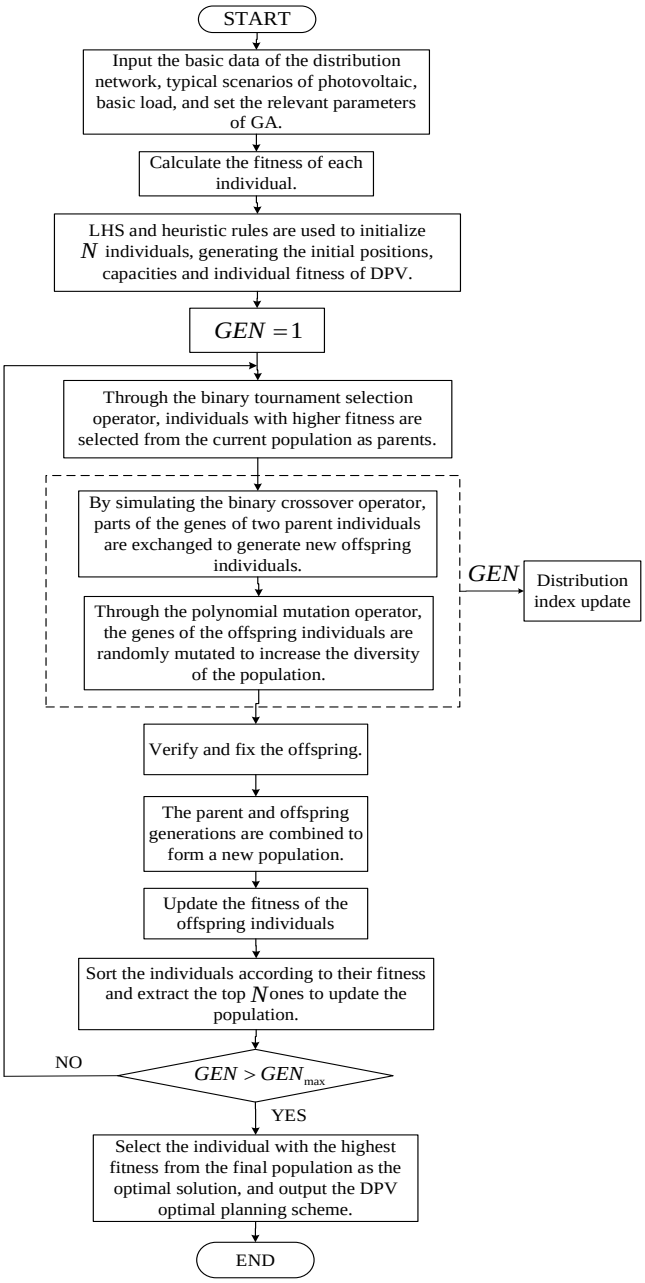

Figure 3: Flowchart of Model Solution

5 Case Study Analysis

5.1 Simulation examples and parameter settings

In the planning model of this paper, the number of installation nodes for DPV is considered to be 3. This paper takes the IEEE-33 node distribution system as an example to verify the proposed planning model. The voltage level of this system is 12.66 kV, and the original load of the system is 7430 + j4600 kVA. The system structure is shown in Figure 4.

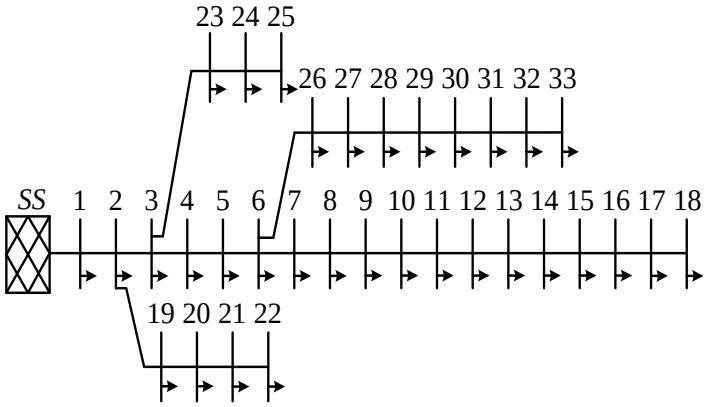

Figure 4: Structure of the IEEE-33 Node Distribution System

The specific parameters of the model are shown in Table 1. In the GA, the location and capacity of the DPV are the decision variables, totaling 6 dimensions [27]. The candidate locations for DPV installation are set as {6, 14, 16, 18, 24, 25, 29, 30, 31, 32}; the maximum number of iterations is set to 30; the population size is set to 50; the crossover probability is set to 0.95; the mutation probability is set to 0.3; and the initial values of the crossover and mutation distribution indices are both set to 20.

Table 1: Model Parameter Settings

Model parameters	numerical value
Electricity selling price / (yuan·kWh^{-1})	0.5
Government's photovoltaic subsidy electricity price / (yuan·kWh^{-1})	0.45
Desulfurization electricity price / (yuan·kWh^{-1})	0.4
Investment cost per unit capacity of DPV / (yuan·kW^{-1})	7850
The operation and maintenance cost per unit capacity of DPV / (yuan·kW^{-1})	0.07
Rated installed capacity of DPV (MW)	0.7
Discount rate	0.06
DPV planning period / years	20
Carbon trading market price / (yuan·t^{-1})	57.5
For every one percentage point improvement in system voltage, the annual revenue gained by power grid enterprises in ensuring user voltage quality / yuan	10000(increase), -50000(reduce)
Carbon dioxide emission coefficient per unit of electricity generated by coal-fired power plants / (kWh·g^{-1})	822.8

5.2 Analysis of Simulation Results

5.2.1 DPV output probability model

Based on the method in Section 1.2, the daily active power output of DPV generated by the LHS technique is shown in Figure 5, with a simulation step of 1 hour and a total of 100 scenarios.

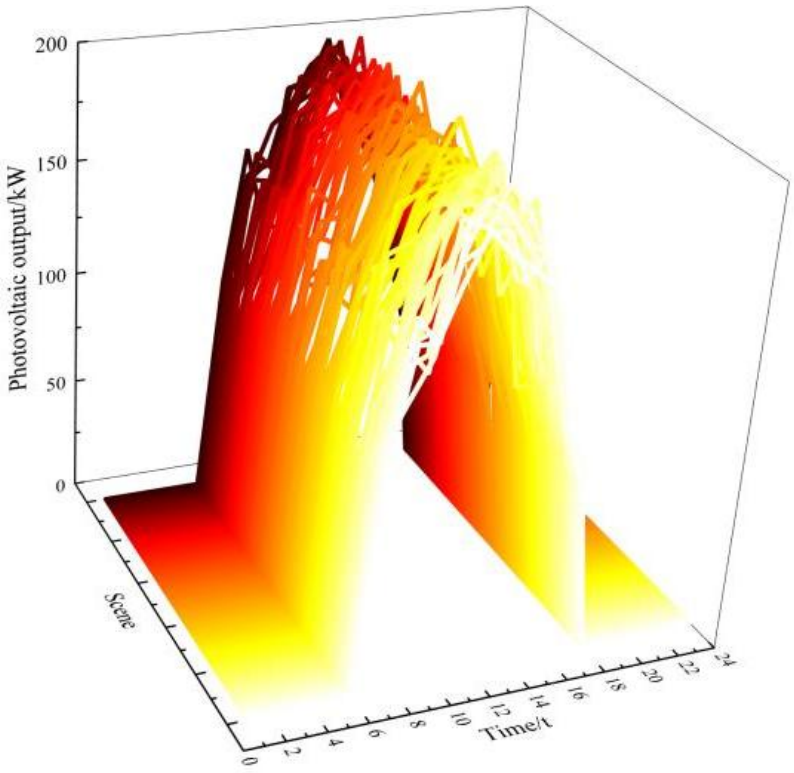

Figure 5: DPV Output Scenarios

As can be seen from Figure 5, the DPV output scenarios generated by the LHS technique cover a variety of DPV output situations. Different weather conditions cause fluctuations in DPV output, and the extent of the fluctuations varies under different circumstances.

Based on the method in Section 1.3, rapid pre-generation reduction was conducted for 100 scenarios. In the same season, the intensity and duration of light present relatively regular periodic fluctuation characteristics [28]. Considering the seasonal differences in DPV output, this paper divides the whole year into three seasons: summer, spring and autumn, and winter. Therefore, the number of reduced scenarios is 3 [29]. The three typical DPV active power output scenarios generated are shown in Figure 6, and the occurrence probabilities of each scenario are 0.288, 0.34, and 0.372.

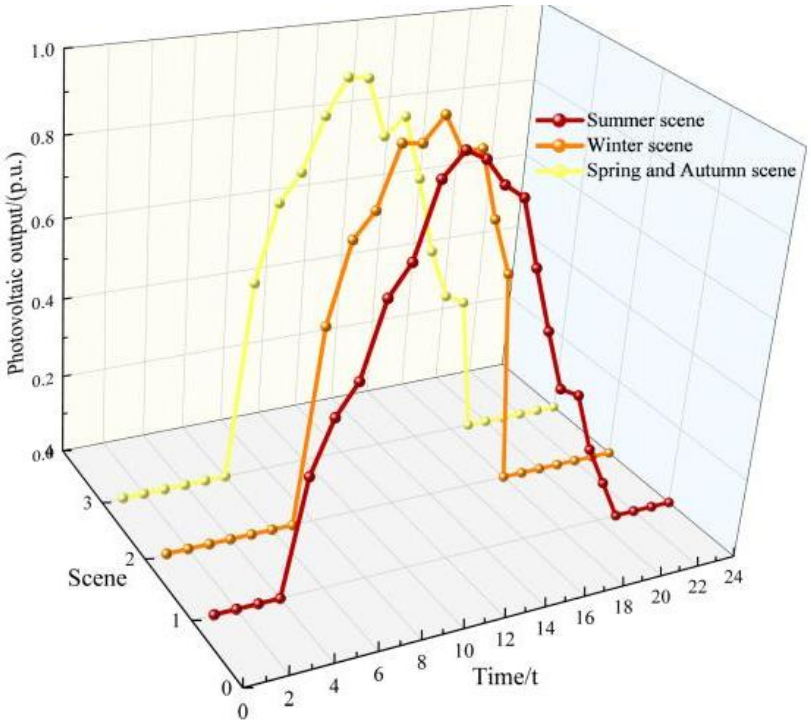

Figure 6: Typical DPV Output Scenarios

5.2.2 Scenario comparison and analysis of DPV site selection and capacity determination

To verify the superiority of considering the system's carbon emission reduction revenue in the comprehensive benefits of the distribution network and the effectiveness of the model proposed in this paper, three scenarios were constructed, among which Scenario 1 is the model established in this paper [30]:

Scenario 1: Maximizing the comprehensive benefits of the distribution network (considering the annual carbon emission reduction revenue), that is $\max C_{DN}$;

Scenario 2: Maximizing the investment returns of DPV-IPP, that is $\max C_{\mathrm{IPP}}$;

Scenario 3: Maximizing the comprehensive benefits of the distribution network (without considering the annual carbon emission reduction revenue), that is $\max(C_{\mathrm{Ploss}} + C_{\mathrm{voltage}})$.

The optimal planning schemes of DPV under different scenarios are shown in Table 2.

Table 2: Optimal Planning Schemes for DPV under Different Scenarios

Scenario	DPV access node/ (installed capacity/kW)	Total installed capacity of DPV / kW	C_{DN}/(ten thousand yuan per year)	Evaluation index/(ten thousand yuan per year)	C_H/(ten thousand yuan per year)	Annual reduction in network loss / MW
Scenario 1	18(649), 24(607), 31(625)	1881	261.16	6.15	42	268.93
Scenario 2	24(700), 25(700), 32(200)	1600	44.28	9.38	30.3	167.22
Scenario 3	18(200), 25(700), 32(648)	1548	200.12	9.06	——	223.82

As can be seen from Table 2, compared with Scenario 1 and Scenario 2, the comprehensive benefit of the distribution network in Scenario 1 is nearly six times higher than that in Scenario 2, and the annual reduction in network losses is 60.8% higher. However, the economic evaluation index in Scenario 1 is 34.4% lower than that in Scenario 2, with a limited gap. The reason for the above results is that in Scenario 2, the investment return of DPV-IPP is the target, and DPV is more inclined to be installed at nodes with smaller loads and closer to power sources to increase the proportion of power fed to the grid and reduce the transmission loss. This layout feature leads to a DPV installation capacity of 1600kW, but the improvement effect on network losses is poor, and the benefit of the distribution network is relatively low. In Scenario 1, the comprehensive benefit of the distribution network is the target, and DPV is installed at nodes 18, 31, etc., which are sensitive to network losses. Although the DPV installation capacity is larger, it somewhat harms the interests of DPV-IPP to some extent. However, due to the better distribution of DPV, the improvement in network losses is significant, and the benefit of the distribution network has been greatly enhanced.

By comparing Scenario 1 and Scenario 3, the annual reduction in network losses in Scenario 1 is 20.2% higher than that in Scenario 3. Even after subtracting the annual carbon emission reduction revenue, the remaining 2.1916 million yuan of the comprehensive distribution network benefits in Scenario 1 is still 190,400 yuan higher than that in Scenario 3. This indicates that when the annual carbon emission reduction revenue is considered in the objective function, the optimization algorithm is more inclined to select nodes with high carbon reduction potential and high sensitivity to network losses. This enables the layout of DPV to enhance the carbon emission reduction revenue while also improving network losses. Therefore, even if the annual carbon emission reduction revenue is excluded, the remaining two parts of the benefits are still superior to those of Scenario 3, which does not include the annual carbon emission reduction revenue. The economic evaluation index of Scenario 1 is 32.1% lower than that of Scenario 3. The reason is that after Scenario 1 introduces the annual carbon emission reduction revenue, the algorithm prioritizes nodes with high power generation, such as nodes 24 and 31, but these nodes have small local loads and mainly generate power for the grid, resulting in a lower economic evaluation index. In contrast, Scenario 3 does not include the annual carbon emission reduction revenue, and the algorithm focuses on network losses and voltage quality, thus choosing nodes with large local loads, such as nodes 25 and 32, where the proportion of self-consumption of generated power is high, leading to a higher economic evaluation index. Therefore, despite the larger installed capacity of DPV in Scenario 1, its economic evaluation index is lower than that of Scenario 3, demonstrating the "side effects" of different optimization objectives on the economic performance of DPV-IPP. This comparison also shows that although the planning scheme for maximizing the comprehensive benefits of the distribution network sacrifices the economic evaluation index, it achieves better improvements in network losses and annual carbon emission reduction revenue, reflecting the comprehensiveness and coordination of the planning objective in Scenario 1.

The voltage distribution curves of the distribution network nodes in the three scenarios of the 12th period are shown in Figure 7.

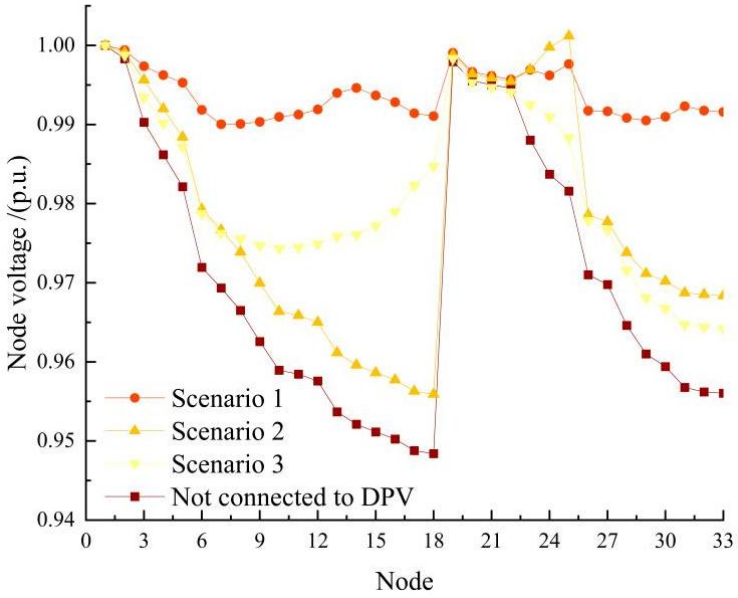

Figure 7: Voltage Distribution Curve at Node in the 12th Time Period

It can be seen that compared with the node voltages of the distribution network without DPV connection, reasonable planning of DPV can effectively increase the system node voltages, and the node voltage quality in Scenario 1 is more ideal. The reason is that the DPV access nodes in Scenario 1 cover the middle and end sections of the line, and the installed capacity at Node 31 is the largest, which significantly improves the voltage at the end section. Meanwhile, the node voltages in Scenario 3 show significant fluctuations. This is because the capacity of Node 25, where DPV is connected, is too large, reaching 700kW, which locally raises the voltage, while the capacity at Node 18 is too small, only 200kW, providing insufficient support at the front end. This indicates that the optimization objective in Scenario 3 lacks guidance on the distribution of DPV capacity, and the layout fails to take into account the overall smoothness of the voltage curve, resulting in a sharp rise followed by a sharp drop in the voltage curve.

6 Conclusion

This paper presents a DPV siting and sizing planning model aimed at maximizing the comprehensive benefits of the distribution network. The investment return of DPV-IPP is taken as the economic evaluation index. The randomness of DPV output is comprehensively considered. LHS and fast forward elimination techniques are adopted to generate typical scenarios, and GA is utilized to jointly optimize the location and capacity of DPV. Through the simulation verification of the IEEE-33 node distribution system, the following conclusions are drawn:

(1) In the process of DPV site selection and capacity planning, considering the randomness of DPV output is more in line with the actual situation and has practical value.

(2) In the process of DPV site selection and capacity planning, incorporating the annual carbon emission reduction revenue into the optimization objective not only directly increases the revenue of the distribution network but also guides the algorithm to choose a DPV layout with more comprehensive benefits.

(3) The planning scheme oriented towards the comprehensive benefits of the distribution network can significantly enhance the operational efficiency of the grid while keeping the loss

of investment return for DPV-IPP within a relatively small range. It achieves a good balance between the comprehensive benefits of the distribution network and the economic viability of DPV-IPP, providing a reference basis for the investment in DPV-IPP and the allowable access locations and capacities of photovoltaic power in the distribution network, which holds practical significance.

Fund Project

This work was supported by State Grid Shandong Electric Power Company Science and Technology Project (520602220004)

Author

Su Hongyu (2000), female, from Yulin, Guangxi, is a master's degree candidate, with research interests in distributed photovoltaic grid connection planning;

Zhang Zhisheng (1975), male, corresponding author, from Qingdao, Shandong, holds a doctorate and is a professor, with research interests in power system load forecasting and economic dispatch.

References

[1] Fard M B, Moradian P, Emarati M, et al. Ground-mounted photovoltaic power station site selection and economic analysis based on a hybrid fuzzy best-worst method and geographic information system: A case study Guilan province[J]. Renewable and Sustainable Energy Reviews, 2022, 169: 112923.

[2] Hasti F, Mamkhezri J, McFerrin R, et al. Optimal solar photovoltaic site selection using geographic information system–based modeling techniques and assessing environmental and economic impacts: The case of Kurdistan[J]. Solar Energy, 2023, 262: 111807.

[3] Abdulmula A, Sopian K, Ludin N A, et al. Micropower system optimization for the telecommunication towers based on various renewable energy sources[J]. International Journal of Electrical and Computer Engineering, 2022, 12(2): 1069.

[4] George D, Venayagamoorthy G K. Digital twins for creating virtual models of solar photovoltaic plants[C]//2023 IEEE symposium series on computational intelligence (SSCI). IEEE, 2023: 252-257.

[5] Villacreses G, Martínez-Gómez J, Jijón D, et al. Geolocation of photovoltaic farms using Geographic Information Systems (GIS) with Multiple-criteria decision-making (MCDM) methods: Case of the Ecuadorian energy regulation[J]. Energy Reports, 2022, 8: 3526-3548.

[6] Ghodusinejad M H, Noorollahi Y, Zahedi R. Optimal site selection and sizing of solar EV charge stations[J]. Journal of Energy Storage, 2022, 56: 105904.

[7] Hassan I, Alhamrouni I, Azhan N H. A CRITIC–TOPSIS multi-criteria decision-making

approach for optimum site selection for solar PV farm[J]. Energies, 2023, 16(10): 4245.

[8] Hosseini P, Taheri S, Akhavan J, et al. Privacy-preserving federated learning: Application to behind-the-meter solar photovoltaic generation forecasting[J]. Energy Conversion and Management, 2023, 283: 116900.

[9] Rekik S, El Alimi S. Optimal wind-solar site selection using a GIS-AHP based approach: a case of Tunisia[J]. Energy Conversion and Management: X, 2023, 18: 100355.

[10] Alhammad A, Sun Q, Tao Y. Optimal solar plant site identification using GIS and remote sensing: framework and case study[J]. Energies, 2022, 15(1): 312.

[11] Raza M A, Yousif M, Hassan M, et al. Site suitability for solar and wind energy in developing countries using combination of GIS-AHP; a case study of Pakistan[J]. Renewable Energy, 2023, 206: 180-191.

[12] Hassan Q, Abdulrahman I S, Salman H M, et al. Techno-economic assessment of green hydrogen production by an off-grid photovoltaic energy system[J]. Energies, 2023, 16(2): 744.

[13] Ali F, Bennui A, Chowdhury S, et al. Suitable site selection for solar-based green hydrogen in southern Thailand using GIS-MCDM approach[J]. Sustainability, 2022, 14(11): 6597.

[14] Zidane T E K, Aziz A S, Zahraoui Y, et al. Grid-connected Solar PV power plants optimization: A review[J]. IEEE Access, 2023, 11: 79588-79608.

[15] Deshmukh A N, Chandrakar V K. Design and performance analysis of grid-connected solar photovoltaic system with performance forecasting approach (PFA)[J]. Journal of The Institution of Engineers (India): Series B, 2022, 103(5): 1521-1532.

[16] Yousefi H, Motlagh S G, Montazeri M. Multi-criteria decision-making system for wind farm site-selection using geographic information system (GIS): Case study of Semnan Province, Iran[J]. Sustainability, 2022, 14(13): 7640.

[17] Mishra S, Saini G, Chauhan A, et al. Optimal sizing and assessment of grid-tied hybrid renewable energy system for electrification of rural site[J]. Renewable Energy Focus, 2023, 44: 259-276.

[18] Massidda L, Bettio F, Marrocu M. Probabilistic day-ahead prediction of PV generation. A comparative analysis of forecasting methodologies and of the factors influencing accuracy[J]. Solar Energy, 2024, 271: 112422.

[19] AlMallahi M N, El Haj Assad M, AlShihabi S, et al. Multi-criteria decision-making approach for the selection of cleaning method of solar PV panels in United Arab Emirates based on sustainability perspective[J]. International Journal of Low-Carbon Technologies, 2022, 17: 380-393.

[20] Visser L, AlSkaif T, van Sark W. Operational day-ahead solar power forecasting for aggregated PV systems with a varying spatial distribution[J]. Renewable Energy, 2022, 183: 267-282.

[21] Mohammad A, Mahjabeen F. Revolutionizing solar energy with ai-driven enhancements in photovoltaic technology[J]. BULLET: Jurnal Multidisiplin Ilmu, 2023, 2(4): 1174-1187.

[22] Zadehbagheri M, Dehghan M, Kiani M, et al. Resiliency-constrained placement and sizing of virtual power plants in the distribution network considering extreme weather events[J]. Electrical Engineering, 2025, 107(2): 2089-2105.

[23] Elboshy B, Alwetaishi M, Aly R M H, et al. A suitability mapping for the PV solar farms in Egypt based on GIS-AHP to optimize multi-criteria feasibility[J]. Ain Shams Engineering Journal, 2022, 13(3): 101618.

[24] Ravichandran N, Ravichandran N, Panneerselvam B. Comparative assessment of offshore floating photovoltaic systems using thin film modules for Maldives islands[J]. Sustainable Energy Technologies and Assessments, 2022, 53: 102490.

[25] Çeçen M, Yavuz C, Tırmıkçı C A, et al. Analysis and evaluation of distributed photovoltaic generation in electrical energy production and related regulations of Turkey[J]. Clean Technologies and Environmental Policy, 2022, 24(5): 1321-1336.

[26] Brester C, Kallio-Myers V, Lindfors A V, et al. Evaluating neural network models in site-specific solar PV forecasting using numerical weather prediction data and weather observations[J]. Renewable Energy, 2023, 207: 266-274.

[27] Saini P, Gidwani L. An investigation for battery energy storage system installation with renewable energy resources in distribution system by considering residential, commercial and industrial load models[J]. Journal of Energy Storage, 2022, 45: 103493.

[28] Panagoda L, Sandeepa R, Perera W, et al. Advancements in photovoltaic (Pv) technology for solar energy generation[J]. J. Res. Technol. Eng, 2023, 4(3): 30-72.

[29] Kumar B A, Jyothi B, Singh A R, et al. Hybrid genetic algorithm-simulated annealing based electric vehicle charging station placement for optimizing distribution network resilience[J]. Scientific Reports, 2024, 14(1): 7637.

[30] Khasanov M, Kamel S, Halim Houssein E, et al. Optimal allocation strategy of photovoltaic-and wind turbine-based distributed generation units in radial distribution networks considering uncertainty[J]. Neural Computing and Applications, 2023, 35(3): 2883-2908.